Geophysical Research Letters

RESEARCH LETTER
10.1029/2024GL111064

Impact of Upper-Plate Faulting on Megathrust Foreshocks: Insights From the 2014 Iquique Earthquake

J. Julve[1], M. Moreno[2], S. Barbot[3], and A. Tassara[1]

[1]Universidad de Concepción, Earth Science Department, Concepcion, Chile, [2]Pontificia Universidad Católica de Chile, Department of Structural and Geotechnical Engineering, Santiago, Chile, [3]University of Southern California, Earth Science Department, Los Angeles, CA, USA

Key Points:

- Offshore upper-plate faulting controls precursory activity of partial megathrust ruptures in Chile
- The hydraulic state at the plate interface impacts precursory seismic activity before megathrust earthquakes

Supporting Information:

Supporting Information may be found in the online version of this article.

Correspondence to:

M. Moreno,
marcos.moreno@uc.cl

Citation:

Julve, J., Moreno, M., Barbot, S., & Tassara, A. (2025). Impact of upper-plate faulting on megathrust foreshocks: Insights from the 2014 Iquique earthquake. *Geophysical Research Letters*, *52*, e2024GL111064. https://doi.org/10.1029/2024GL111064

Received 3 JUL 2024
Accepted 18 DEC 2024

Author Contributions:

Conceptualization: J. Julve, M. Moreno
Methodology: J. Julve, S. Barbot
Supervision: M. Moreno, S. Barbot
Visualization: J. Julve
Writing – original draft: J. Julve
Writing – review & editing: M. Moreno, S. Barbot, A. Tassara

Abstract The role of upper-plate faulting in the seismic cycle of large megathrust earthquakes remains poorly understood. We use quasi-dynamic numerical simulations of seismic cycles to analyze the interaction between crustal faulting and the foreshock sequence of the 2014 Iquique (Mw 8.2) earthquake in Northern Chile. Multi-cycle models incorporating upper-plate faulting align better with coseismic displacements, replicating events akin to the Iquique earthquake. Upper-plate faulting significantly influences foreshock seismicity and deformation patterns. By calibrating the average hydraulic state—varying the effective normal stress—along the megathrust with pre-earthquake seismicity, we find that lower pore pressure ratios result in more seismicity before the mainshock. This implies that the hydraulic state of the megathrust is critical for foreshock activity. This comprehensive modeling approach underscores the importance of the mechanical interplay between the megathrust and upper-plate faults in precursory sequences of large subduction zone earthquakes.

Plain Language Summary Active upper-plate faults in subduction zones worldwide have shown activity before, during, and after large earthquakes, suggesting a link with megathrust behavior. Advancing our understanding of these mechanisms is essential for enhancing seismic hazard assessment. The 2014 Iquique earthquake (Mw 8.2) in Northern Chile is probably the best-documented earthquake in terms of pre-earthquake upper-plate activity, characterized by an intense foreshock sequence 15 days before the main event. Here, we use numerical simulations of the seismic cycle over several thousand years to analyze the interaction between crustal faulting and foreshocks preceding events like the 2014 Iquique earthquake. Upper-plate faults in our models significantly influence the seismic activity prior to the mainshock and are key to explaining the geodetic observations of coseismic displacements. Additionally, we find that the hydraulic state at the plate interface strongly affects foreshock activity. This research highlights the importance of fault interactions and fluid dynamics in the seismic cycles of subduction zones.

1. Introduction

Upper-plate faults are found above the seismogenic megathrusts in subduction zones worldwide (e.g., Barnes et al., 2002; Melnick et al., 2009; Schurr et al., 2014; Wilson et al., 2006), with evidence of synchronized activity between these fault systems, as observed before (Hayes et al., 2014; Schurr et al., 2014), during (Herman et al., 2023; Melnick et al., 2012), and after large subduction zone earthquakes (Farias et al., 2011; Fukushima et al., 2018; Kato et al., 2011). The mechanical coupling between the megathrust and offshore upper-plate faults produces transient slip, leading to earthquake clustering and aseismic slip (Ruiz et al., 2014), and enhances tsunami excitation in the outer wedge (Qiu & Barbot, 2022). However, the mechanisms controlling the triggering, delay, and size of earthquakes among upper-plate faults fracturing the outer wedge are still poorly understood. Dynamic models suggest that the permanent deformation of the upper plate accumulates over the seismic cycle (Sathiakumar et al., 2020, 2024; van Dinther et al., 2014; van Zelst et al., 2022). This fault-related forearc deformation can redistribute stress and pore fluid pressure (Wang et al., 2019), affecting megathrust dynamics.

On 1 April 2014, a magnitude (Mw) 8.1 megathrust earthquake struck the subduction zone in Northern Chile close to Iquique (Figure 1a). The mainshock was preceded by a slow-slip event that began 8 months earlier (Socquet et al., 2017) and was intensified by a sequence of foreshocks starting on 16 March 2014, with a Mw 6.7 event that ruptured an offshore west-dipping upper plate fault (Bedford et al., 2015; González et al., 2015; Ruiz et al., 2014; Schurr et al., 2014; Soto et al., 2019) (Figures 1a and 1b). Pre-earthquake seismicity migrated toward the updip

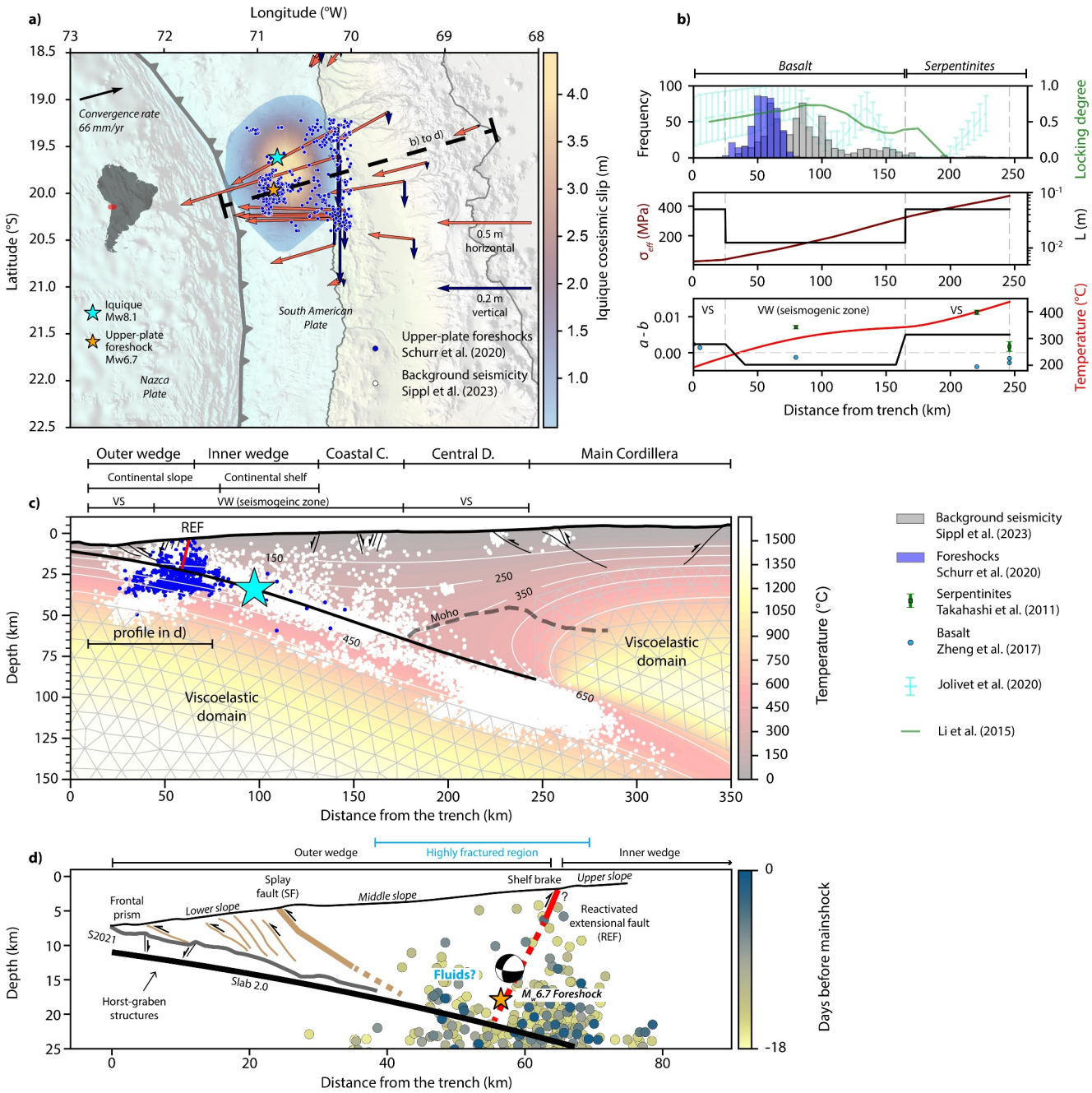

Figure 1. Tectonic setting, model structure, and forearc features. (a) Coseismic slip distribution of the 2014 Iquique earthquake (Schurr et al., 2014). GNSS-derived displacements indicate consistent horizontal deformation toward the area of maximum slip (red vectors) and coastal subsidence (black vectors). The foreshock sequence (blue dots) increased after the occurrence of a Mw 6.7 upper-plate fault earthquake (orange star) 15 days before the mainshock. The foreshocks and the mainshock epicenter (cyan star) surround the zone of maximum coseismic slip. (b) Top: Distributions of background (gray) and foreshock (blue) seismicity and locking degree. Foreshocks in the histogram are filtered to show only those interpreted as interplate events. Center: Distributions of effective stress ($\bar{\sigma}$) and values of parameter *L*. (c) White and blue dots are background and foreshock seismicity. Bottom: Distribution of parameters a and b, which frictionally segment the velocity-strengthening (VS) and velocity-weakening (VW) behavior of the megathrust. The slab temperatures from our thermal model and the rocks at the plate interface are shown. Coastal C. = Coastal Cordillera, Central D. = Central Depression. Upper-plate structure based on the works of Storch et al. (2021), Geersen et al. (2018), and Giambiagi et al. (2022). The dashed line is the Moho discontinuity from Comte et al. (2016). White contours are isotherms from our temperature distribution. Gray triangles represent the mesh of the viscoelastic domain. (d) The faults in red and brown are interpreted according to Storch et al. (2021), from which we also obtained the bathymetry and the plate interface (line S2021).

portion of the locked region of the plate interface (Schurr et al., 2020; Socquet et al., 2017), suggesting a mechanical interaction between an offshore west-dipping fault at the eastern limit of the outer wedge and the megathrust (Herman et al., 2016; Schurr et al., 2020). Decoupling and aseismic slip on the plate interface following the seismic activity in the upper-plate (González et al., 2015; Herman et al., 2016) may have driven the northward migration of the foreshocks that culminated 15 days later with the large Mw 8.1 mainshock (Meng et al., 2015; Ruiz et al., 2014). Nevertheless, unraveling the influence of hanging-wall structures on seismicity at the plate interface remains a recondite problem.

Here, we use quasi-dynamic numerical simulations of multiple seismic cycles to examine the mechanical interactions between a west-dipping offshore upper-plate fault and the megathrust, resembling the structural context of the Iquique 2014 earthquake. We establish a two-dimensional modeling framework integrating geological and geophysical data to assess the mechanical role of an active upper-plate fault in the initiation of large megathrust earthquakes. We compare our models with seismic activity during the pre-seismic unrest phase of the Iquique sequence and with geodetic data during the coseismic displacement. Our analysis suggests that an offshore west-dipping upper-plate fault influences the precursory phase of megathrust earthquakes, where a reduction in pore pressure ratio within the seismogenic zone drives foreshock activity.

2. Data and Methods

2.1. Modeling Upper-Plate Fault and Megathrust Earthquake Cycles

We investigate how an offshore upper-plate fault influences megathrust earthquakes in Northern Chile, using 2D quasi-dynamic models to assess its impact on rupture and precursory activity in subduction zones. We estimate the evolution of slip-rate over time using UniCyclE (Barbot, 2018, 2020) and a slip-rate- and state-dependent friction law under isothermal and isobaric conditions (Barbot, 2019a). We use the Slab2 model (Hayes et al., 2018) to constrain the megathrust geometry. Foreshock seismicity 1 month before the Mw 8.1 Iquique earthquake (Schurr et al., 2020), seismic line interpretations of the forearc structure (Storch et al., 2021), and the preferred orientation of nodal planes from the Mw 6.7 earthquake (Herman et al., 2016; Schurr et al., 2020) delineate the offshore fault (Figure 1c, Supplementary Figure 4 in Supporting Information S1). We determine the temperature distribution using a finite element method (Araya et al., 2023), considering a stratified continental plate with constant thermal properties. Further model details are given in Supplementary Materials S1 to S4 in Supporting Information S1.

We infer the distribution of frictional parameters at the plate interface in Northern Chile based on geological and geophysical data. Our cross-section at 20°S incorporates subduction zone features by integrating seismic tomography, reflection profiles (Comte et al., 2016; Geersen et al., 2018; Sallarès & Ranero, 2005; Storch et al., 2021), foreshock seismicity before the Mw 8.1 Iquique earthquake (Schurr et al., 2020), geodetic locking models (Jolivet et al., 2020; Li et al., 2015), and a new thermal model (Figure 1b, Supplementary Material S4 in Supporting Information S1). The Northern Chile subduction zone has a thin sedimentary layer resulting in a narrow frontal accretionary prism of 5–30 km in the outer wedge (Geersen et al., 2018; Maksymowicz et al., 2018) (Figure 1c). Seismicity (Schurr et al., 2020; Sippl et al., 2023; Soto et al., 2019) and locking models (Jolivet et al., 2020; Li et al., 2015) indicate frictional instability along the megathrust from 17 to 60 km depth. The outer wedge shows intense faulting and high *Vp/Vs* ratios, suggesting a high-fluid zone (Petersen et al., 2021, Figure 1d).

Seismic wave profiles show a lack of sediments in the trench, indicating that the oceanic plate is interacting directly with the upper plate, with the frictional contact dominated by basaltic rocks (Geersen et al., 2015) (Figure 1b). We use the mean a and b values controlling the direct and steady-state velocity dependence of friction (Supplementary Material S1 in Supporting Information S1, Equation 1) from laboratory experiments on basalt gouges (Zhang et al., 2017) (Figure 1b), defining a velocity-strengthening region below the outer wedge (<100°C) and a velocity-weakening domain between the inner wedge and the Coastal Cordillera (100°C–300°C, Figures 1b and 1c). At greater depths, seismic wave *Vp/Vs* ratios indicate serpentinization in the cold mantle wedge (Comte et al., 2016). Therefore, we assume that serpentinites control the frictional behavior at that depth and take the frictional parameters a and b from laboratory experiments on lizardite and antigorite (D. E. Moore & Lockner, 2011; Okazaki & Katayama, 2015; Takahashi et al., 2011). The steady-state velocity-strengthening behavior of serpentinites at temperatures below 450°C (Figures 1b and 1c) is consistent with the transition

from high locking degree areas (>0.5), and with the end of the background seismicity (Figure 1b). Frictional parameters are summarized in Supplementary Material Table 2 in Supporting Information S1.

We compute the effective normal stress (Figure 1b) $\overline{\sigma} = (1 - \lambda)\sigma_n$, assuming an average background pore fluid pressure ratio $\lambda = 0.825$. This value closely aligns with the mean value explaining strain rates observed in the rock fabrics in paleo-subduction zones, ranging between brittle creep and solution precipitation creep as deformation mechanisms (Oncken et al., 2021). The outer and inner wedge regions exhibit background and foreshock seismicity, indicating a highly fractured environment (Herman et al., 2016; Soto et al., 2019; Storch et al., 2021, Figure 1d), with densities consistent with a mafic composition (Sallarès & Ranero, 2005; Tassara & Echaurren, 2012). Sedimentary sequences are primarily confined to the poorly developed frontal accretionary prism and the slope of the forearc wedge (Geersen et al., 2018). We infer that the offshore upper-plate fault associated with the foreshock sequence, cut through upper crust mafic rocks. The minimum depth of seismicity indicates velocity weakening from 5 km depth. We assume the same a and b values as those used for the seismogenic megathrust (Figure 1b), ignoring the narrow sedimentary cover beneath the middle and lower slopes. The characteristic slip distance L, representing the slip needed to return to steady state after a velocity perturbation (Rice, 1993), is chosen (Figure 1b) to resolve nucleation size and capture simulated seismicity on both faults.

3. Results and Discussion

3.1. Slip Mechanisms

We consider two end-member simulations. The first model (M1, Figure 2a) assumes that the megathrust is the only active fault, while the second model (M2, Figures 1d–2b) also incorporates an active west-dipping offshore upper-plate fault. For the megathrust, the loading rate $V_L = 67$ mm/yr comes from the relative convergence velocity (Figure 1a). For the upper plate fault, we assume that this structure accommodates 20% of the local plate convergence (Sathiakumar et al., 2020), resulting in $V_L = 13.4$ mm/yr. Due to modeling constraints, we assume that the offshore west-dipping upper-plate fault has reverse kinematics throughout the subduction seismic cycle. Although dynamic models (Herrera et al., 2023) and Coulomb wedge theory (Wang et al., 2019; Wang & Hu, 2006) suggest that normal faulting can occur on westward-dipping structures during the coseismic phase, we focus on the latter part of the interseismic phase preceding Iquique-like earthquakes, where a reverse mechanism is expected, as evidenced by the Mw 6.7 upper-plate event on 15 March 2014. Each simulation spans 5,000 years, excluding the first 3,000 years to reduce the influence of initial conditions.

In both M1 and M2 simulations, the seismic cycles exhibit a series of earthquakes with different rupture lengths (Figure 2). Full ruptures extend from the down-dip limit of the seismogenic zone up to the trench, while partial ruptures occur at the upper and lower parts of the velocity weakening region (Figures 2a and 2b). Each partial earthquake is followed by a sequence of aftershocks located at the tip of each rupture, which then cascade into a new event, leading to a precursory phase for another earthquake (Figures 2a and 2b). The upper portion of the megathrust seismogenic zone experiences extended periods of acceleration, which in some cases can be classified as slow-slip events ($10^{-8} < V < 10^{-7}$ m/s), lasting decades before a new partial earthquake occurs (Figures 2a and 2b). This acceleration is accompanied by either pulse-like (Figure 2a) or progressive (Figure 2b) unlocking of the velocity-weakening segment, generated by the differences of prescribed convergence rate above the intersection between both faults. The down-dip area is characterized by intense seismicity, represented by foreshock sequences lasting hundreds of years, which limit the size of subsequent down-dip partial ruptures (Figures 2a and 2b).

In simulation M1, a supercycle of partial and full ruptures lasts about 800 years (Figure 2a), while in M2, the duration spans around 750 years (Figure 2b). To determine the magnitude of these events, we employ a scaling law that correlates the maximum coseismic slip (MCS) with Mw (Brengman et al., 2019). We recover the maximum slip of each event reaching a slip rate greater than 1 mm/s (Figures 2a and 2b). For M1 and M2, the MCS of full ruptures reaches maximum values of 54.9 and 52.2 m, respectively. We then apply (Brengman et al., 2019):

$$M_w = 6.3574 + 1.5439\ log(MCS) \quad (1)$$

As a result, a Mw 9 is obtained for both cases, consistent with estimates of the magnitude of the last giant earthquake in 1877 (Mw > 8.5) (Vigny & Klein, 2022). For the updip partial earthquakes, the rupture process

10.1029/2024GL111064

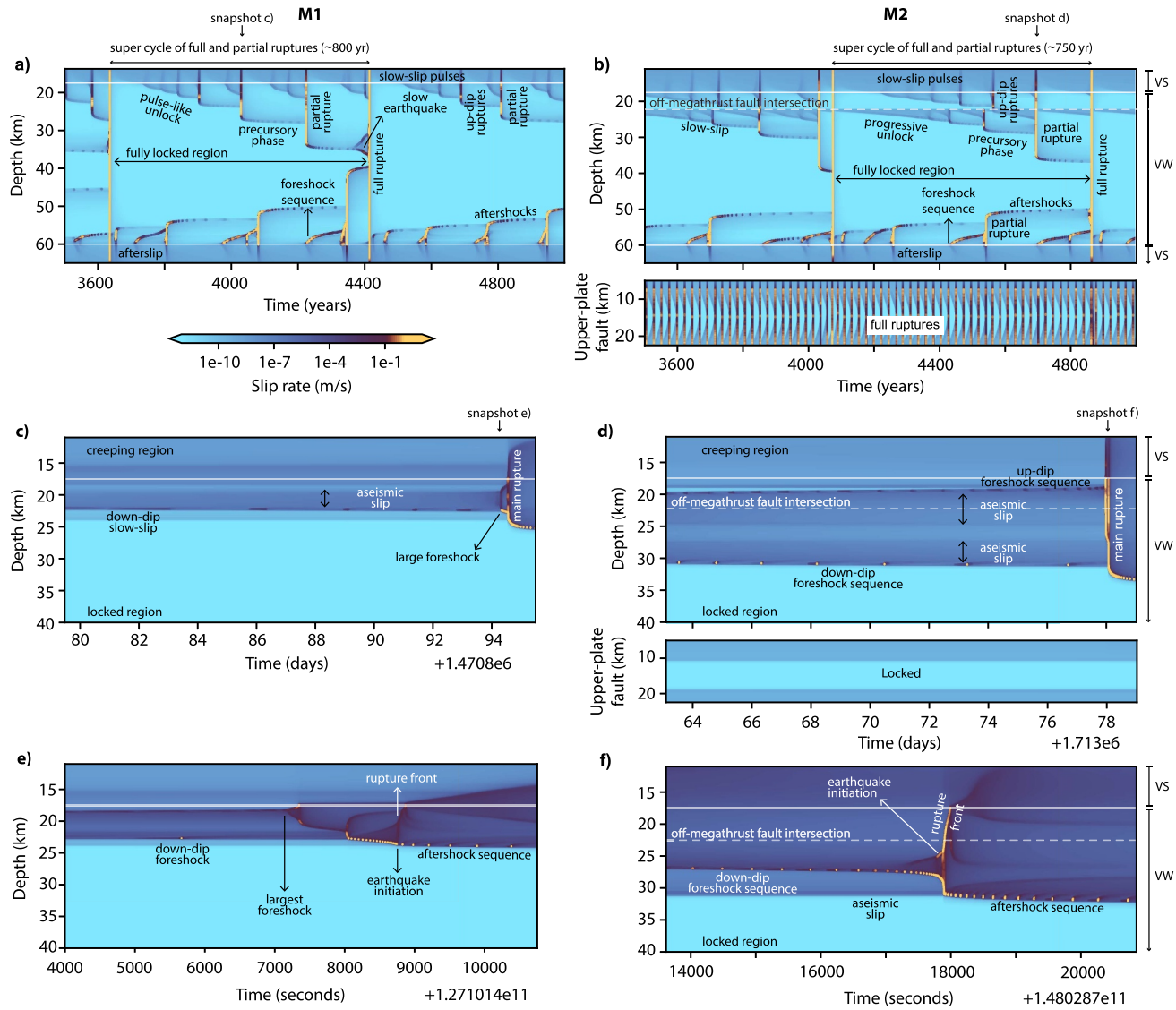

Figure 2. Slip-rate over time and rupture styles during a 1,500-year of seismic cycle. (a) Supercycle of full and partial ruptures for M1. Yellow lines represent a megathrust earthquake. White lines are the limits of the velocity weakening (VW) region defined in Figure 1b. The supercycle lasts 800 years. Full ruptures are the ones that break from the trench up to the down-dip velocity strengthening (VS) area. Partial ruptures break a portion of the velocity-weakening region and can be nucleated at the updip or down-dip limit within the seismogenic zone. (b) Same as in (a) but for M2. The lower panel of (b) presents the evolution of slip-rate in the upper-plate fault at the same time as in the megathrust. (c) and (d) describe the slip-rate and seismic activity 16 days before each mainshock, while (e) and (f) show the same but 2 hr before the main rupture.

initiates at the updip limit of the foreshock activity (Figures 2e and 2f) and then propagates up to the boundary of the velocity-strengthening region and down to a point within the seismogenic zone (Figures 2e and 2f), resembling the Mw 8.1 Iquique earthquake. Both the updip and down-dip foreshock sequences are accompanied by aseismic slip, accelerating the fault within the rupture length (Figures 2c–2f). Upon initiation, the earthquake rupture front progresses toward the updip limit between the velocity-weakening and velocity-strengthening regions, ultimately diffusing at this boundary (Figures 2e and 2f). Applying Equation 1, the maximum simulated partial earthquakes in M1 reach MCS = 9.2 m and Mw 7.8, while in M2 MCS = 11.9 m and Mw 8.0 (Figures 3e and 3f).

Both models exhibit similar rupture patterns (Figures 2a and 2b) that arise from the elevated Dieterich-Ruina-Rice number R_u (Barbot, 2019b) that controls the importance of non-local stress transfer and results from the frictional

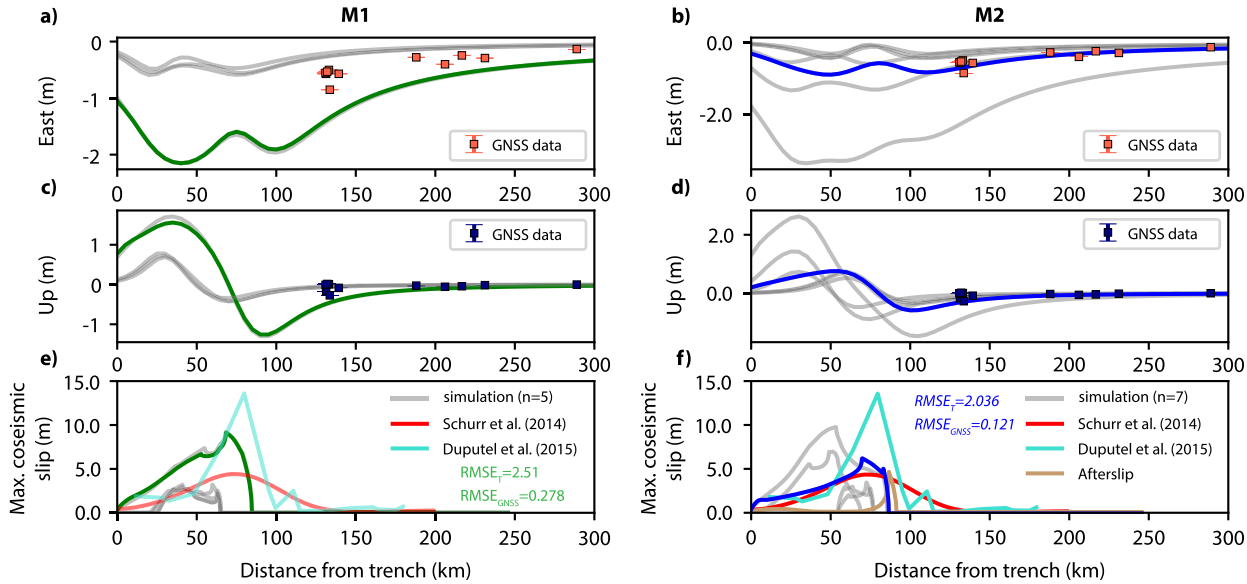

Figure 3. GNSS data and kinematic coseismic slip model of the Iquique earthquake versus model results. In both M1 and M2, the blue and green lines represent the partial rupture event with lowest $RMSE_T$ from each model. The n value represents all the simulated partial ruptures from each model. (a) and (b) show the eastward GNSS coseismic displacements (orange-red squares) for the Iquique earthquake and the simulated displacements (gray and colored lines) by partial ruptures. (c) and (d) show the GNSS vertical coseismic displacements of the Iquique earthquake i (blue squares), and the displacements simulated by partial ruptures (gray and colored lines). (e) and (f) show two different coseismic slip models for the Iquique earthquake from Schurr et al. (2014) and Duputel et al. (2015), and all the simulated coseismic slips from the partial ruptures generated by the model along with afterslip of the best model.

configuration and the geometry of the system. In our modeling, the megathrust has a minimum value of $R_u = 195.3$ within the velocity weakening region, which is associated with down-dip and updip partial ruptures, and full rupture of the seismogenic zone (Barbot, 2019b). In addition, M2 shows a clear influence of the upper-plate fault on the precursory activity prior to the main partial rupture (Figures 2d and 2f), developing a combination of aseismic slip and foreshock seismicity at the megathrust weeks before the mainshock. Given the assumed R_u number, updip partial events in Northern Chile may be linked to the gouge composition at the plate interface and to the length of the seismogenic zone, factors known to affect the rupture style and recurrence patterns within the velocity-weakening region (Barbot, 2019b; Nie & Barbot, 2022).

Recurrence times scales with (b-a), $\overline{\sigma}$, and the length of the seismogenic zone (Veedu Mele & Barbot, 2016), resulting in full length seismic ruptures that repeat approximately every 11 years for the upper-plate fault, with MCS = 0.403 m and Mw 5.8. Since (b-a) and $\overline{\sigma}$ are constrained by geological observations, to capture the full spectrum of seismic activity will require smaller values of L (e.g., $L < 1$ mm), which will dramatically increase the computational workload. As a result and having $R_u = 8.2$, we are unable to capture the complete foreshock sequence of low-amplitude seismicity observed before the Iquique mainshock (Figures 1c and 1d).

3.2. Surface Deformation

To verify our results with observations, we compute the root mean squared error ($RMSE$) between GNSS-derived displacements (see Supplementary Material S5 in Supporting Information S1) and our modeling outputs in two cases: first, comparing the coseismic displacement from the GNSS data with the simulated surface deformation ($RMSE_{GNSS}$ Figures 3e and 3f); and second, assessing the combined difference between GNSS data plus coseismic slip (Duputel et al., 2015; Schurr et al., 2014) against the same model results ($RMSE_T$ Figures 3e and 3f). In both cases, M2 exhibits a better fit to the data than M1 (Figure 3), suggesting that Iquique-like events are better explained when an offshore upper-plate fault is active and mechanically coupled with the megathrust.

M1 generates two families of partial ruptures: the first with no more than 0.5 m of surface displacements in the east and vertical components; and the second with larger deformation reaching 2 m of westward motion and 1.5 m

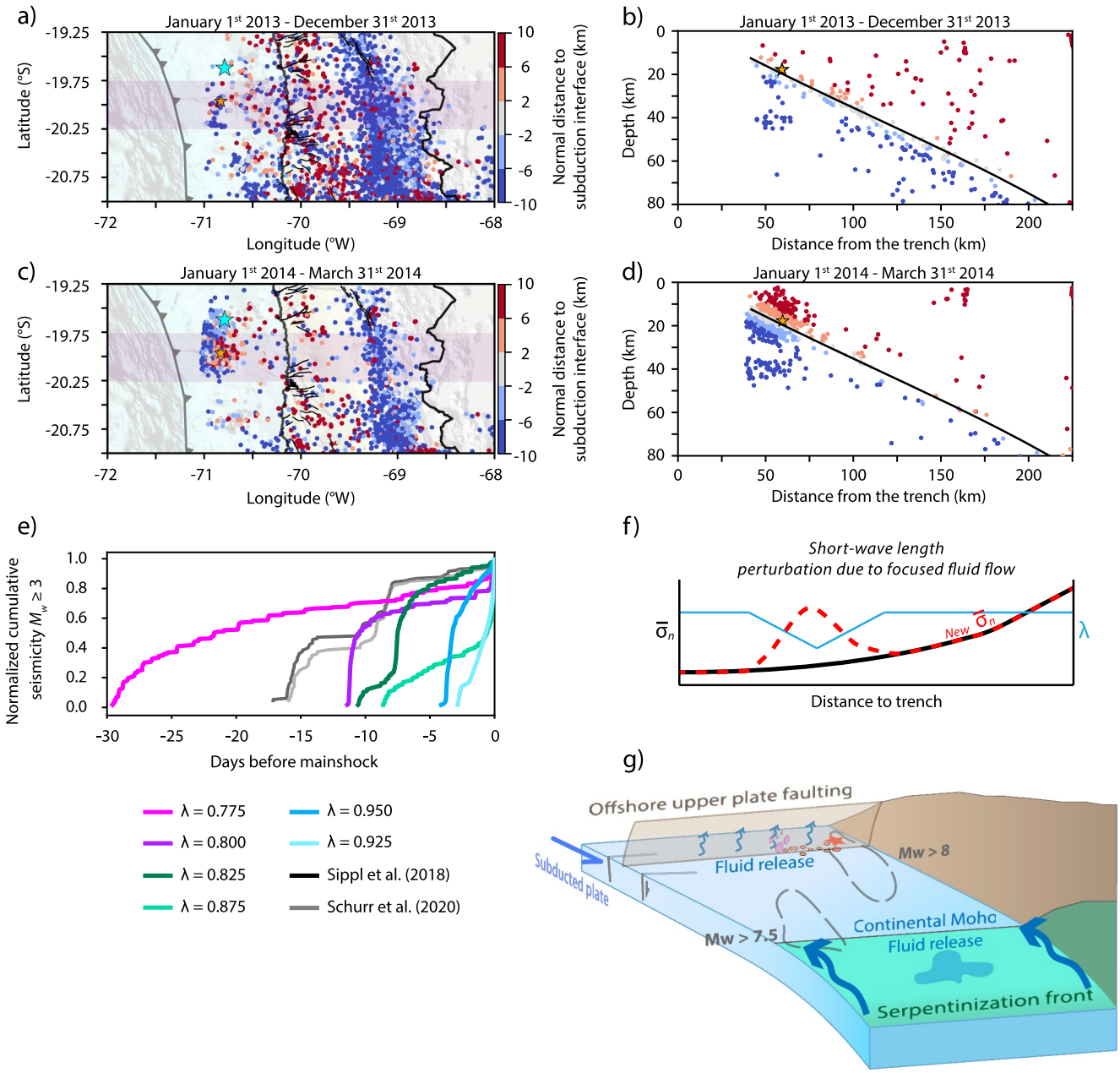

Figure 4. Foreshock seismicity and conceptual model. (a) to (d) correspond to the catalog of Sippl et al. (2023). The purple box represents the area at which we select the seismicity for the cross sections in (b) and (d). (e) foreshock seismicity is normalized for the total number of events before each mainshock. (f) illustrates a schematic representation of the short-wavelength perturbation that best represents the observations. (g) Depicts a conceptual model of the hydraulic relationship between the offshore upper-plate fault and the megathrust. Pink and orange circles are precursory seismicity prior to the mainshock (red star).

of coseismic uplift offshore, along with 1.25 m of subsidence near the coast (Figures 3a and 3c). The $RMSE_T = 2.51$ m with a maximum slip of 9.2 m (Figure 3e).

M2 also exhibits two families of partial ruptures. Larger events reach a maximum of 2.5 and 3 m of offshore uplift and westward motion respectively, with coastal subsidence of 1.9 m. The event with the lowest $RMSE_T$ (blue line Figures 3b–3d and 3f) shows 0.8 m of westward motion and offshore uplift, with coastal subsidence of 0.7 m (Figures 3b and 3d). The coseismic slip has a maximum of 5 m, which is the same value obtained by Schurr et al. (2014), but lower than the 13 m estimated by Duputel et al. (2015) (Figure 3f). The afterslip is confined below 60 km depth (Figure 3f), as observed with geodetic data for the Iquique earthquake (Itoh et al., 2023). In M2, the event with maximum coseismic slip is close to the results obtained by Duputel et al. (2015) and has a

Mw closer to the 2014 Iquique earthquake. Also, it reproduces better the position of the rupture termination close to 100 km from the trench (Figure 3f).

3.3. Precursory Activity and Changes in Effective Normal Stress

Since M2 can better explain surface deformation and precursory activity prior to updip partial ruptures, we use it to explore the role of pore-fluid pressure on the development of seismicity. Foreshock activity on the plate interface may have been triggered by seismic unrest in the upper plate (e.g., Schurr et al., 2020). A sudden increase in seismicity in the upper plate observed months before the mainshock (Figures 4a–4d) suggests the causative role of fluids. To test this hypothesis, we explore how changes in pore-fluid pressure control the distribution of seismicity during this period. We compute the moment magnitude of each simulated foreshock (Figure 2f) and obtain the normalized cumulative seismicity 1 month before the mainshock. We then compare this to the foreshock seismicity observed in the same period before the Iquique event (Mw > 3, Figure 4e). We consider a realistic distribution of pore fluid pressure based on thermodynamic calculations (Condit et al., 2020, Supplementary Figure 3 in Supporting Information S1). Our results show that when pore fluid pressure perturbations decrease, the frequency and timing of foreshocks increase (Figure 4e). A decrease in pore fluid pressure leads to an increase in $\overline{\sigma}$ and thus in R_u. Nucleation size decrease, leading to an enhancement in smaller ruptures.

We suggest that the hydraulic state, prior to an updip partial rupture, is controlled by focused fluid flow from the megathrust up to the upper-plate (Figures 4f and 4g, e.g., Sun et al., 2020). Mineral vein growth (e.g., Fagereng, 2011; Fagereng & Harris, 2014), solution-precipitation creep (e.g., Brantut et al., 2011; Rowe et al., 2011; Vannucchi & Leoni, 2007), pressure solution and fault healing (e.g., Gratier et al., 2013, 2014), fluid-pressurization (e.g., Taetz et al., 2017; French & Condit, 2019; Tarling et al., 2019), and fault valving (e.g., Sibson, 1992; Zhu et al., 2020), highlight the role of pore fluid pressure evolution with time. While we assumed a constant distribution of $\overline{\sigma}$ over time in our model, preventing us from accounting for these mechanisms in detail, our approach is a first step in identifying that, at a first-order level, down-dip gradients in pore fluid pressure are necessary to generate the observed foreshock pattern and upper plate activation.

4. Conclusions

Using quasi-dynamic numerical models of the Northern Chile subduction zone, our study reveals the complex interplay between slip mechanisms driven by the interaction of the megathrust with west-dipping upper-plate faults located offshore, between the inner and outer wedge. Both full and partial ruptures exhibit distinct precursory phases characterized by foreshock seismicity and aseismic slip, followed by intense aftershock sequences. While the occurrence of updip partial ruptures like the Iquique 2014 event is not directly influenced by upper-plate faulting, their presence significantly impacts the rate of foreshock seismicity and surface deformation patterns. Models integrating offshore upper-plate faults show better alignment with observed data, particularly in replicating events akin to the Iquique earthquake, underscoring the mechanical interaction between these structures and the megathrust. Furthermore, our exploration of changes in effective normal stress along the subduction zone demonstrates that lower pore fluid pressure increases foreshock activity before partial ruptures, providing valuable insights into the mean hydraulic state within the megathrust, which governs the initiation of seismicity culminating in large earthquakes. This study highlights the critical role of comprehensive modeling in understanding fault interactions and their role in generating precursory activity, such as foreshocks, and emphasizes the importance of fluid-rock interactions during the later stages of the interseismic phase in megathrust seismic cycles.

Conflict of Interest

The authors declare no conflicts of interest relevant to this study.

Data Availability Statement

The code for quasi-dynamic modeling - UniCyclE - can be found at: https://bitbucket.org/sbarbot/unicycle/src/master/. The input parameters for each simulation M1 and M2, the effective normal stress distributions used to model different scenarios of Figure 4, the coseismic displacements derived from data of the GPS stations, the thermal model at 20°S, and the codes to process the output from UniCyclE (Figure 3) can be found at (Julve

et al., 2024): https://doi.org/10.5281/zenodo.12615565. Foreshock seismicity was obtained from the work of Sippl et al. (2018) (https://doi.org/10.1002/2017JB015384), Sippl et al. (2023) (https://doi.org/10.1016/j.jsames.2023.104326), and Schurr et al. (2020) (https://doi.org/10.1029/2020GL088351).

Acknowledgments
This work is supported by the National Agency of Research and Development (ANID-Human Resources Branch/National Doctorate/2021-21211844) (J.J) and by the FONDECYT project 1221507 and 1240862 (M.M). S.B is funded by the National Science Foundation under award number EAR-1848192. M.M. acknowledges support from Instituto Milenio de Oceanografía AIM23-0003.

References

Araya, R., Cárcamo, C., & Poza, A. H. (2023). A stabilized finite element method for the Stokes–Temperature coupled problem. *Applied Numerical Mathematics*, *187*, 24–49. https://doi.org/10.1016/j.apnum.2023.02.002

Barbot, S. (2018). Asthenosphere flow modulated by megathrust earthquake cycles. *Geophysical Research Letters*, *45*(12), 6018–6031. https://doi.org/10.1029/2018GL078197

Barbot, S. (2019a). Modulation of fault strength during the seismic cycle by grain-size evolution around contact junctions. *Tectonophysics*, *765*, 129–145. https://doi.org/10.1016/j.tecto.2019.05.004

Barbot, S. (2019b). Slow-slip, slow earthquakes, period-two cycles, full and partial ruptures, and deterministic chaos in a single asperity fault. *Tectonophysics*, *768*, 228171. https://doi.org/10.1016/j.tecto.2019.228171

Barbot, S. (2020). Frictional and structural controls of seismic super-cycles at the Japan trench. *Earth Planets and Space*, *72*(1), 63. https://doi.org/10.1186/s40623-020-01185-3

Barnes, P. M., Nicol, A., & Harrison, T. (2002). Late Cenozoic evolution and earthquake potential of an active listric thrust complex above the Hikurangi subduction zone, New Zealand. *GSA Bulletin*, *114*(11), 1379–1405. https://doi.org/10.1130/0016-7606(2002)114<1379:LCEAEP>2.0.CO;2

Bedford, J., Moreno, M., Schurr, B., Bartsch, M., & Oncken, O. (2015). Investigating the final seismic swarm before the Iquique-Pisagua 2014 M_w 8.1 by comparison of continuous GPS and seismic foreshock data. *Geophysical Research Letters*, *42*(10), 3820–3828. https://doi.org/10.1002/2015GL063953

Brantut, N., Han, R., Shimamoto, T., Findling, N., & Schubnel, A. (2011). Fast slip with inhibited temperature rise due to mineral dehydration: Evidence from experiments on gypsum. *Geology*, *39*(1), 59–62. https://doi.org/10.1130/g31424.1

Brengman, C. M. J., Barnhart, W. D., Mankin, E. H., & Miller, C. N. (2019). Earthquake-scaling relationships from Geodetically derived slip distributions. *Bulletin of the Seismological Society of America*, *109*(5), 1701–1715. https://doi.org/10.1785/0120190048

Comte, D., Carrizo, D., Roecker, S., Ortega-Culaciati, F., & Peyrat, S. (2016). Three-dimensional elastic wave speeds in the northern Chile subduction zone: Variations in hydration in the supraslab mantle. *Geophysical Journal International*, *207*(2), 1080–1105. https://doi.org/10.1093/gji/ggw318

Condit, C. B., Guevara, V. E., Delph, J. R., & French, M. E. (2020). Slab dehydration in warm subduction zones at depths of episodic slip and tremor. *Earth and Planetary Science Letters*, *552*, 116601. https://doi.org/10.1016/j.epsl.2020.116601

Duputel, Z., Jiang, J., Jolivet, R., Simons, M., Rivera, L., Ampuero, J.-P., et al. (2015). The Iquique earthquake sequence of April 2014: Bayesian modeling accounting for prediction uncertainty. *Geophysical Research Letters*, *42*(19), 7949–7957. https://doi.org/10.1002/2015GL065402

Fagereng, Å. (2011). Fractal vein distributions within a fault-fracture mesh in an exhumed accretionary mélange, Chrystalls Beach Complex, New Zealand. *Journal of Structural Geology*, *33*(5), 918–927. https://doi.org/10.1016/j.jsg.2011.02.009

Fagereng, Å., & Harris, C. (2014). Interplay between fluid flow and fault–fracture mesh generation within underthrust sediments: Geochemical evidence from the Chrystalls Beach Complex, New Zealand. *Tectonophysics*, *612*, 147–157. https://doi.org/10.1016/j.tecto.2013.12.002

Farías, M., Comte, D., Roecker, S., Carrizo, D., & Pardo, M. (2011). Crustal extensional faulting triggered by the 2010 Chilean earthquake: The Pichilemu Seismic Sequence. *Tectonics*, *30*(6), TC6010. https://doi.org/10.1029/2011TC002888

French, M. E., & Condit, C. B. (2019). Slip partitioning along an idealized subduction plate boundary at deep slow slip conditions. *Earth and Planetary Science Letters*, *528*, 115828. https://doi.org/10.1016/j.epsl.2019.115828

Fukushima, Y., Toda, S., Miura, S., Ishimura, D., Fukuda, J., Demachi, T., & Tachibana, K. (2018). Extremely early recurrence of intraplate fault rupture following the Tohoku-Oki earthquake. *Nature Geoscience*, *11*(10), 777–781. https://doi.org/10.1038/s41561-018-0201-x

Geersen, J., Ranero, C., Barckhausen, U., & Reichert, C. (2015). Subducting seamounts control interplate coupling and seismic rupture in the 2014 Iquique earthquake area. *Nature Communications*, *6*(1), 8267. https://doi.org/10.1038/ncomms9267

Geersen, J., Ranero, C. R., Klaucke, I., Behrmann, J. H., Kopp, H., Tréhu, A. M., et al. (2018). Active tectonics of the north Chilean marine forearc and adjacent oceanic Nazca plate. *Tectonics*, *37*(11), 4194–4211. https://doi.org/10.1029/2018TC005087

Giambiagi, L., Tassara, A., Echaurren, A., Julve, J., Quiroga, R., Barrionuevo, M., et al. (2022). Crustal anatomy and evolution of a subduction-related orogenic system: Insights from the Southern Central Andes (22-35 S). *Earth-Science Reviews*, *232*, 104138. https://doi.org/10.1016/j.earscirev.2022.104138

González, G., Salazar, P., Loveless, J. P., Allmendinger, R. W., Aron, F., & Shrivastava, M. (2015). Upper plate reverse fault reactivation and the unclamping of the megathrust during the 2014 northern Chile earthquake sequence. *Geology*, *43*(8), 671–674. https://doi.org/10.1130/G36703.1

Gratier, J.-P., Dysthe, D. K., & Renard, F. (2013). Chapter 2 - The role of pressure solution creep in the ductility of Earth's upper crust. *Advances in Geophysics*, *54*, 47–179. https://doi.org/10.1016/B978-0-12-380940-7.00002-0

Gratier, J. P., Renard, F., & Vial, B. (2014). Postseismic pressure solution creep: Evidence and time-dependent change from dynamic indenting experiments. *Journal of Geophysical Research: Solid Earth*, *119*(4), 2764–2779. https://doi.org/10.1002/2013jb010768

Hayes, G., Herman, M., Barnhart, W., Furlong, K. P., Riquelme, S., Benz, H. M., et al. (2014). Continuing megathrust earthquake potential in Chile after the 2014 Iquique earthquake. *Nature*, *512*(7514), 295–298. https://doi.org/10.1038/nature13677

Hayes, G. P., Moore, G. L., Portner, D. E., Hearne, M., Flamme, H., Furtney, M., & Smoczyk, G. M. (2018). Slab2, a comprehensive subduction zone geometry model. *Science*, *362*(6410), 58–61. https://doi.org/10.1126/SCIENCE.AAT4723/SUPPL_FILE/AAT4723-HAYES-SM.PDF

Herman, M. W., Furlong, K. P., & Benz, H. M. (2023). Substantial upper plate faulting above a shallow subduction megathrust earthquake: Mechanics and implications of the surface faulting during the 2016 Kaikoura, New Zealand, earthquake. *Tectonics*, *42*(5), e2022TC007645. https://doi.org/10.1029/2022TC007645

Herman, M. W., Furlong, K. P., Hayes, G. P., & Benz, H. M. (2016). Foreshock triggering of the 1 April 2014 Mw 8.2 Iquique, Chile, earthquake. *Earth and Planetary Science Letters*, *447*, 119–129. https://doi.org/10.1016/j.epsl.2016.04.020

Herrera, M. T., Crempien, J. G. F., & Cembrano, J. (2023). Complex crustal deformation controlled by the 3D geometry of the Chile subduction zone. *Bulletin of the Seismological Society of America*, *113*(6), 2479–2491. https://doi.org/10.1785/0120230062

Itoh, Y., Socquet, A., & Radiguet, M. (2023). Largest aftershock nucleation driven by afterslip during the 2014 Iquique sequence. *Geophysical Research Letters*, *50*(24). https://doi.org/10.1029/2023gl104852

Jolivet, R., Simons, M., Duputel, Z., Olive, J.-A., Bhat, H. S., & Bletery, Q. (2020). Interseismic loading of subduction megathrust drives long-term uplift in Northern Chile. *Geophysical Research Letters*, *47*(8), e2019GL085377. https://doi.org/10.1029/2019GL085377

Julve, J., Moreno, M., Barbot, S., & Tassara, A. (2024). Impact of Upper-Plate Faulting on megathrust foreshocks: Insights from the 2014 Iquique earthquake. *Zenodo*. [Dataset]. https://doi.org/10.5281/zenodo.12615565

Kato, A., Sakai, S., & Obara, K. (2011). A normal-faulting seismic sequence triggered by the 2011 off the Pacific coast of Tohoku Earthquake: Wholesale stress regime changes in the upper plate. *Earth Planets and Space*, *63*(7), 745–748. https://doi.org/10.5047/eps.2011.06.014

Li, S., Moreno, M., Bedford, J., Rosenau, M., & Oncken, O. (2015). Revisiting viscoelastic effects on interseismic deformation and locking degree: A case study of the Peru-north Chile subduction zone. *Journal of Geophysical Research: Solid Earth*, *120*(6), 4522–4538. https://doi.org/10.1002/2015JB011903

Maksymowicz, A., Ruiz, J., Vera, E., Contreras-Reyes, E., Ruiz, S., Arraigada, C., et al. (2018). Heterogeneous structure of the Northern Chile marine forearc and its implications for megathrust earthquakes. *Geophysical Journal International*, *215*(2), 1080–1097. https://doi.org/10.1093/gji/ggy325

Melnick, D., Bookhagen, B., Strecker, M. R., & Echtler, H. P. (2009). Segmentation of megathrust rupture zones from fore-arc deformation patterns over hundreds to millions of years, Arauco peninsula, Chile. *Journal of Geophysical Research*, *114*(B1), B01407. https://doi.org/10.1029/2008JB005788

Melnick, D., Moreno, M., Motagh, M., Cisternas, M., & Wesson, R. L. (2012). Splay fault slip during the Mw 8.8 2010 Maule Chile earthquake. *Geology*, *40*(3), 251–254. https://doi.org/10.1130/G32712.1

Meng, L., Huang, H., Bürgmann, R., Ampuero, J. P., & Strader, A. (2015). Dual megathrust slip behaviors of the 2014 Iquique earthquake sequence. *Earth and Planetary Science Letters*, *411*, 177–187. https://doi.org/10.1016/j.epsl.2014.11.041

Moore, D. E., & Lockner, D. A. (2011). Frictional strengths of talc-serpentine and talc-quartz mixtures. *Journal of Geophysical Research*, *116*(B1), B01403. https://doi.org/10.1029/2010JB007881

Nie, S., & Barbot, S. (2022). Rupture styles linked to recurrence patterns in seismic cycles with a compliant fault zone. *Earth and Planetary Science Letters*, *591*, 117593. https://doi.org/10.1016/j.epsl.2022.117593

Okazaki, K., & Katayama, I. (2015). Slow stick slip of antigorite serpentinite under hydrothermal conditions as a possible mechanism for slow earthquakes. *Geophysical Research Letters*, *42*(4), 1099–1104. https://doi.org/10.1002/2014GL062735

Oncken, O., Angiboust, S., & Dresen, G. (2021). Slow slip in subduction zones: Reconciling deformation fabrics with instrumental observations and laboratory results. *Geosphere*, *18*(1), 104–129. https://doi.org/10.1130/GES02382.1

Petersen, F., Lange, D., Ma, B., Grevemeyer, I., Geersen, J., Klaeschen, D., et al. (2021). Relationship between subduction erosion and the up-dip limit of the 2014 Mw 8.1 Iquique earthquake. *Geophysical Research Letters*, *48*(9). https://doi.org/10.1029/2020GL092207

Qiu, Q., & Barbot, S. (2022). Tsunami excitation in the outer wedge of global subduction zones. *Earth-Science Reviews*, *230*, 104054. https://doi.org/10.1016/j.earscirev.2022.104054

Rice, J. R. (1993). Spatio-temporal complexity of slip on a fault. *Journal of Geophysical Research*, *98*(B6), 9885–9907. https://doi.org/10.1029/93jb00191

Rowe, C. D., Meneghini, F., & Moore, J. C. (2011). Textural record of the seismic cycle: Strain-rate variation in an ancient subduction thrust. *Geological Society*, *359*(1), 77–95. https://doi.org/10.1144/sp359.5

Ruiz, S., Metois, M., Fuenzalida, A., Ruiz, J., Leyton, F., Grandin, R., et al. (2014). Intense foreshocks and a slow slip event preceded the 2014 Iquique M_w 8.1 earthquake. *Science*, *345*(6201), 1165–1169. https://doi.org/10.1126/science.1256074

Sallarès, V., & Ranero, C. R. (2005). Structure and tectonics of the erosional convergent margin off Antofagasta, north Chile (23°30′S). *Journal of Geophysical Research*, *110*(B6). https://doi.org/10.1029/2004JB003418

Sathiakumar, S., Barbot, S., & Hubbard, J. (2020). Earthquake cycles in fault-bend folds. *Journal of Geophysical Research: Solid Earth*, *125*(8), e2019JB018557. https://doi.org/10.1029/2019JB018557

Sathiakumar, S., Barbot, S., & Hubbard, J. (2024). The role of fault structural evolution on long-term slip rates and seismic cycles in the Himalayan orogenic wedge. *Earth and Planetary Science Letters*, *630*, 118599. https://doi.org/10.1016/j.epsl.2024.118599

Schurr, B., Asch, G., Hainzl, S., Bedford, J., Hoechner, A., Palo, M., et al. (2014). Gradual unlocking of plate boundary controlled initiation of the 2014 Iquique earthquake. *Nature*, *512*(7514), 299–302. https://doi.org/10.1038/nature13681

Schurr, B., Moreno, M., Tréhu, A. M., Bedford, J., Kummerow, J., Li, S., & Oncken, O. (2020). Forming a Mogi Doughnut in the Years prior to and immediately before the 2014 *M* 8.1 Iquique, northern Chile, earthquake. *Geophysical Research Letters*, *47*(16). https://doi.org/10.1029/2020GL088351

Sibson, R. H. (1992). Fault-valve behavior and the hydrostatic-lithostatic fluid pressure interface. *Earth-Science Reviews*, *32*(1–2), 141–144. https://doi.org/10.1016/0012-8252(92)90019-p

Sippl, C., Schurr, B., Münchmeyer, J., Barrientos, S., & Oncken, O. (2023). The Northern Chile forearc constrained by 15 years of permanent seismic monitoring. *Journal of South American Earth Sciences*, *126*, 104326. https://doi.org/10.1016/j.jsames.2023.104326

Sippl, C., Schurr, B., Asch, G., & Kummerow, J. (2018). Seismicity structure of the northern Chile forearc from >100,000 double-difference relocated hypocenters. *Journal of Geophysical Research: Solid Earth*, *123*(5), 4063–4087. https://doi.org/10.1002/2017jb015384

Socquet, A., Valdes, J. P., Jara, J., Cotton, F., Walpersdorf, A., Cotte, N., et al. (2017). An 8 month slow slip event triggers progressive nucleation of the 2014 Chile megathrust. *Geophysical Research Letters*, *44*(9), 4046–4053. https://doi.org/10.1002/2017GL073023

Soto, H., Sippl, C., Schurr, B., Kummerow, J., Asch, G., Tilmann, F., et al. (2019). Probing the northern Chile megathrust with seismicity: The 2014 M8.1 Iquique earthquake sequence. *Journal of Geophysical Research: Solid Earth*, *124*(12), 12935–12954. https://doi.org/10.1029/2019JB017794

Storch, I., Buske, S., Victor, P., & Oncken, O. (2021). Seismic images of the Northern Chilean subduction zone at 19°40′S, prior to the 2014 Iquique earthquake. *Geophysical Journal International*, *225*(2), 1048–1061. https://doi.org/10.1093/gji/ggab035

Sun, T., Ellis, S., & Saffer, D. (2020). Coupled evolution of deformation, pore fluid pressure, and fluid flow in shallow subduction forearcs. *Journal of Geophysical Research: Solid Earth*, *125*(3), e2019JB019101. https://doi.org/10.1029/2019JB019101

Taetz, S., John, T., Bröcker, M., Spandler, C., & Stracke, A. (2017). Fast fluid-flow events within a subduction-related vein system in oceanic eclogite: Implications for pore fluid pressure at the plate interface. In *EGU general assembly conference abstracts*.12617.

Takahashi, M., Uehara, S.-I., Mizoguchi, K., Shimizu, I., Okazaki, K., & Masuda, K. (2011). On the transient response of serpentine (antigorite) gouge to stepwise changes in slip velocity under high-temperature conditions. *Journal of Geophysical Research*, *116*(B10), B10405. https://doi.org/10.1029/2010JB008062

Tarling, M. S., Smith, S. A., & Scott, J. M. (2019). Fluid overpressure from chemical reactions in serpentinite within the source region of deep episodic tremor. *Nature Geoscience*, *12*(12), 1034–1042. https://doi.org/10.1038/s41561-019-0470-z

Tassara, A., & Echaurren, A. (2012). Anatomy of the Andean subduction zone: Three-dimensional density model upgraded and compared against global-scale models. *Geophysical Journal International*, *189*(1), 161–168. https://doi.org/10.1111/j.1365-246X.2012.05397.x

van Dinther, Y., Mai, P. M., Dalguer, L. A., & Gerya, T. V. (2014). Modeling the seismic cycle in subduction zones: The role and spatiotemporal occurrence of off-megathrust earthquakes. *Geophysical Research Letters*, *41*(4), 1194–1201. https://doi.org/10.1002/2013GL058886

Vannucchi, P., & Leoni, L. (2007). Structural characterization of the Costa Rica décollement: Evidence for seismically-induced fluid pulsing. *Earth and Planetary Science Letters*, *262*(3–4), 413–428. https://doi.org/10.1016/j.epsl.2007.07.056

van Zelst, I., Rannabauer, L., Gabriel, A.-A., & van Dinther, Y. (2022). Earthquake rupture on multiple splay faults and its effect on tsunamis. *Journal of Geophysical Research: Solid Earth*, *127*(8), e2022JB024300. https://doi.org/10.1029/2022JB024300

Veedu, D. M., & Barbot, S. (2016). The Parkfield tremors reveal slow and fast ruptures on the same asperity. *Nature*, *532*(7599), 361–365. https://doi.org/10.1038/nature17190

Vigny, C., & Klein, E. (2022). The 1877 megathrust earthquake of north Chile two times smaller than thought? A review of ancient articles. *Journal of South American Earth Sciences*, *117*, 103878. https://doi.org/10.1016/j.jsames.2022.103878

Wang, K., Brown, L., Hu, Y., Yoshida, K., He, J., & Sun, T. (2019). Stable forearc stressed by a weak megathrust: Mechanical and geodynamic implications of stress changes caused by the M = 9 Tohoku-oki earthquake. *Journal of Geophysical Research: Solid Earth*, *124*(6), 6179–6194. https://doi.org/10.1029/2018JB017043

Wang, K., & Hu, Y. (2006). Accretionary prisms in subduction earthquake cycles: The theory of dynamic Coulomb wedge. *Journal of Geophysical Research*, *111*(B6). https://doi.org/10.1029/2005JB004094

Wilson, K., Berryman, K., Litchfield, N., & Little, T. (2006). A revision of mid-late Holocene marine terrace distribution and chronology at the Pakarae River mouth, North Island, New Zealand. *New Zealand Journal of Geology and Geophysics*, *49*(4), 477–489. https://doi.org/10.1080/00288306.2006.9515182

Zhang, L., He, C., Liu, Y., & Lin, J. (2017). Frictional properties of the South China Sea oceanic basalt and implications for strength of the Manila subduction seismogenic zone. *Marine Geology*, *394*, 16–29. https://doi.org/10.1016/j.margeo.2017.05.006

Zhu, W., Allison, K. L., Dunham, E. M., & Yang, Y. (2020). Fault valving and pore pressure evolution in simulations of earthquake sequences and aseismic slip. *Nature Communications*, *11*(1), 4833. https://doi.org/10.1038/s41467-020-18598-z